

Article

Numerical Investigation on the Effects of Baffles with Various Thermal and Geometrical Conditions on Thermo-Fluid Dynamics and Kinetic Power of a Solar Updraft Tower

Seungjin Lee ¹, Yoon Seok Kim ² and Joong Yull Park ^{1,2,*} 

¹ Department of Mechanical Engineering, Graduate School, Chung-Ang University, 84 Heukseok-ro, Dongjak-gu, Seoul 06974, Republic of Korea; leesj09@cau.ac.kr

² Department of Mechanical System Engineering, Graduate School, Chung-Ang University, 84 Heukseok-ro, Dongjak-gu, Seoul 06974, Republic of Korea; kys0618asd@cau.ac.kr

* Correspondence: jrpark@cau.ac.kr; Tel.: +82-2-820-5888

Received: 20 July 2018; Accepted: 22 August 2018; Published: 25 August 2018



Abstract: Solar updraft towers (SUTs) are used for renewable power generation, taking advantage of the thermal updraft air flow caused by solar energy. Aerodynamic devices have been applied to SUTs to improve their performance and the baffle is one such device. Here, we investigate the effect of baffle installation on the thermo-fluid dynamic phenomena in the collector of an SUT and how it enhances the overall SUT performance using computational fluid dynamics analysis. Two geometric parameters (height and width of baffle) and two thermal boundary conditions of the baffle (adiabatic condition and heat flux condition) were tested through simulations with 10 different models. The vortex generated by the baffle has a positive effect on the delivery of heat energy from the ground to the main flow; however, one disadvantage is that the baffle inherently increases the resistance of the main flow. Over 3% higher kinetic power was achieved with some of the simulated baffle models. Therefore, an optimum design for baffle installation can be achieved by considering the positive and negative thermo-fluid dynamics of baffles.

Keywords: solar updraft tower (SUT); baffle; computational fluid dynamics (CFD); vortex; kinetic power; heat transfer

1. Introduction

Non-renewable energy sources, represented by fossil fuels, cannot meet the growing demand for energy in the future, not only because of its limited supply but also because it significantly disrupts the ecosystem [1]. For this reason, there has been growing interest in renewable energy sources. In particular, solar energy, which is the most abundant energy on Earth, is expected to be one of the most suitable renewable energy sources to replace conventional fossil fuels [2]. A solar updraft tower (SUT) power plant is one means to convert solar energy into electrical energy generated by buoyancy-driven air flow [3]. An SUT power plant consists of three main parts: a collector, chimney and wind turbine (Figure 1a). In the collector, thermal energy from solar radiant energy transfers heat to the ground. The air near the ground is heated and density differences in the flow occur due to temperature gradients, which is a natural convection phenomenon. The buoyancy force due to the density differences acts as a driving force to generate the flow in the SUT. The kinetic power of this air flow is converted into electric energy by the wind turbine mounted inside the SUT.

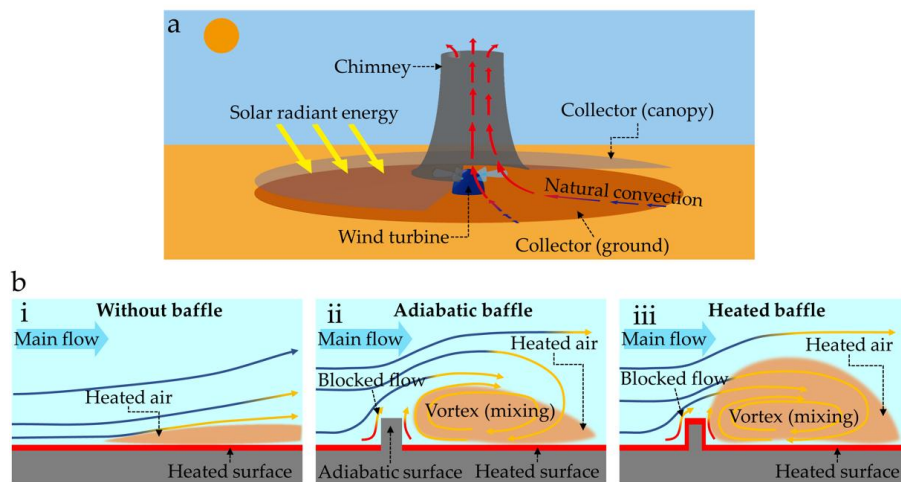


Figure 1. Schematic of a solar updraft tower (SUT) and flow phenomenon near the baffle. (a) Composition and operating principle of the SUT. The SUT consists of a collector, chimney and wind turbine. (b) Schematic of the flow around the baffle inside the SUT according to the baffle thermal boundary conditions. (i) Flow field in the Conv_SUT without a baffle. (ii) Flow field in the downstream of the baffle under adiabatic condition. (iii) Flow field in the downstream of the baffle under heat flux condition.

SUTs have been developed and discussed as a type of large-scale power plant [3–6]. Since the first prototype was built in 1982 [7–9], research on SUTs has been more actively pursued [3]. To improve SUT performance, several studies on the application of aerodynamic design have been carried out. Some of these studies have shown that the performance of SUTs varies according to their geometric parameters. The effect of the height and diameter of the collector outlet and chimney throat diameter on SUT performance has been reported to determine the aerodynamically optimized design [10–12]. An analytical and numerical study to optimize the collector inlet and chimney height showed that the influence of the chimney diameter is greater than that of the chimney height [13]. Five design parameters (collector radius, collector inlet height, collector outlet height, chimney height and diameter) that affect system performance were simultaneously optimized for the system efficiency, power output and system expenditure [14]. Numerical investigations on canopy slopes and chimney geometries (heights and angles) have been conducted [15–17]. Five canopy shapes including new geometries (segmented and stepped profile) were studied to confirm the aerodynamic performance of each design [18]. Some other studies have attempted to increase efficiency by applying a diffuser-shaped chimney to the SUT to create lower static pressure regions near the chimney outlet in order to increase the pressure difference and thus the flow rate [10,16,19].

In a broad perspective, the abovementioned studies have focused on increasing the flow of the SUT by improving the general SUT shape, which serves as a casing for the internal flow. At the same time, compared with the overall design of the SUT, microperspective research has been performed to improve SUT performance through local thermal-fluidic improvement. Some studies have focused on aerodynamic devices and components in the flow paths of SUTs. There have been studies on the inlet guide vane, an aerodynamic component already used in turbomachinery, to guide the flow into the wind turbine at the transition region of the chimney and collector of an SUT [20–22]. The guide wall, located in the collector-to-chimney transition region like the inlet guide vane, was studied by considering the mechanical functions of mounting the wind turbine and guiding/directing the air flowing horizontally in the collector toward the vertical direction in the chimney [23].

Additionally, we noted a previous study of an obstacle placed at the SUT collector ground to interfere with the flow in the SUT [24]. The study reported that the obstacle (baffle) improved SUT performance due to the enhanced mixing caused by the vortex that formed downstream of the obstacle.

It should be noted that this principle is frequently considered in industrial heat exchanger designs using various shapes, such as fin, baffle, vortex generator and so forth, to increase heat transfer efficiency [25–34]. The key point in this heat exchanger design is to take into consideration both the negative aspect of increased flow resistance that arises from the installation of the obstacle and the positive aspect of heat transfer enhancement to the vortex as mentioned above. As a result, the in-depth analysis of the above-mentioned positive and negative aspects of obstacle installation is required. However, few studies on the SUT have explored this concept/method.

In this work, we used a numerical method to investigate the effects of diverse baffle geometries on SUT performance. In an SUT collector with a baffle, higher temperature distribution was observed compared with that of a conventional SUT (Conv_SUT) without a baffle, which resulted in increased kinetic power of the SUT. We focused on two baffle effects: the influence of heat transfer area increased by the area of the baffle and the flow formation due to the presence of a baffle (the reduction of collector cross-section of the flow path and the vortex downstream of the baffle). Three types of SUTs were considered to observe the effects of baffles (Figure 1b). In the Conv_SUT without a baffle, simple flow was created by natural convection without the interference of a baffle (Figure 1b–i). In the SUT with an adiabatic baffle, a negative effect due to the decreased cross-section of the flow path and a positive effect of the mixing of heated air and the main flow due to the vortex that occurred downstream of baffle, were observed (Figure 1b–ii). In an SUT with a heated baffle, another advantage is the additional heat surface area of the baffle that increases the heat supply to the main flow (Figure 1b–iii). For these three examples, a case study of baffle height and width was performed to confirm the effect of baffle size. An analysis was conducted through observation of the streamline and temperature distribution and the kinetic power of these cases was also compared.

2. Materials and Methods

In the simulations, the collector radius of the SUT, total height, collector inlet height and chimney exit diameter were 5 m, 13 m, 0.15 m and 0.25 m, respectively (Figure 2a), for which 2D axisymmetric geometry was applied for computation. The baffle was located at the bottom of the SUT (Figure 2b–i). The position of the baffle was 2 m from the axis and the case study was conducted to predict the baffle effect according to the height (H) and width (W) (Figure 2b–ii). A total of 10 models were constructed using nine different combinations of baffle heights and widths and thermal conditions (adiabatic or heated surface). The Conv_SUT without a baffle was used as a control. The smallest baffle, which was 0.1 m in height and 0.08 m in width, was called H10. Based on this model, other models with 1.5, 2 and 2.5 times the baffle height and width were used in the case study (Table 1). Flow field and temperature distribution analysis of the SUTs was performed using ANSYS Fluent 17.0 (ANSYS, Inc., Canonsburg, PA, US), a commercial computational fluid dynamics (CFD) package.

Our computational models assumed steady-state turbulent flow for which the standard $k-\varepsilon$ model was used because of its proven accuracy in predicting the temperature profile of the SUT collectors in earlier studies [35–38]. In addition, the enhanced wall treatment was applied to resolve the laminar sublayer near the wall [39]. See the ‘Supplementary Materials’ for further detailed description on the flow dynamics model used in this study. Air was used as the working fluid and the density and thermal expansion coefficient of air are 1.1543 kg/m^3 and $3.2805 \times 10^{-3} \text{ K}^{-1}$, respectively. To realize natural convection, the Boussinesq model was applied [40]. In the process of calculating the buoyancy force, which is the driving force of natural convection, this Boussinesq model treats the density as a constant value in the governing equations except for the buoyancy term of the momentum equation. Because of the simplicity of density calculations, this method provides better convergence than using an ideal gas model or incompressible ideal gas model. The density of the buoyancy term in the momentum equation is determined by followed equation:

$$(\rho - \rho_0)g \approx -\rho_0\beta(T - T_0)g, \quad (1)$$

where ρ_0 is the constant density of the working fluid, β is the thermal expansion coefficient and T_0 is the operating temperature. The inlet boundary condition is a pressure inlet condition of 1 atm with temperature of 300 K. The outlet boundary condition is a pressure outlet condition of 1 atm with temperature of 300 K. For the thermal boundary conditions, the heat emitted from the ground collector due to solar heat was assumed to be 13 W/m^2 and the walls of the canopy of the collector and chimney were assumed to be adiabatic. The operating conditions 1 atm (101,325 Pa) and 288.16 K were used. The abovementioned numerical methods and conditions are summarized in Table 2.

Table 1. Nine models with different dimensions of baffles.

Model Name	Height (m)	Width (m)	Baffle Condition
H-models	H10_A	0.08	Adiabatic
	H10_Q		Heated
	H15_A		Adiabatic
	H15_Q		Heated
	H20_A		Adiabatic
	H20_Q		Heated
W-models	W15_Q	0.12	Heated
	W20_Q	0.16	Heated
	W25_Q	0.2	Heated

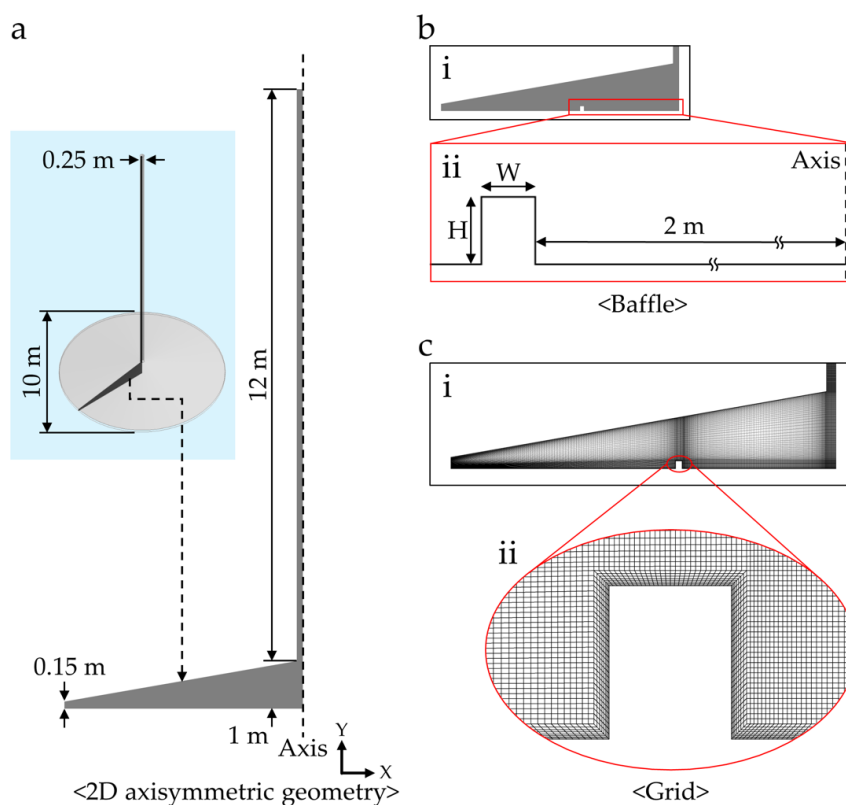


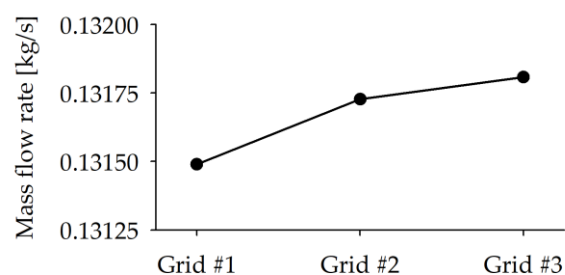
Figure 2. Computation domain and grid. (a) 2D axisymmetric geometry without a baffle. (b) Baffle position; (i) geometry with baffle and (ii) baffle shape parameters (H: baffle height, W: baffle width). (c) Computational grid; (i) grid system of geometry with baffle and (ii) grid around baffle with inflation layer (dense grid on the surface).

Table 2. Numerical method and condition.

Numerical Method	
Time	Steady state
Turbulence model	Standard k- ϵ
Wall function	Enhanced wall treatment
Grid number	125,727
Operating condition	
Operating pressure	1 atm
Operating temperature	288.16 K
Working fluid (air)	
Density	Boussinesq model (1.1543 kg/m ³)
Thermal expansion coefficient	$3.2805 \times 10^{-3} \text{ K}^{-1}$
Boundary condition	
Inlet	1 atm, 300 K
Outlet	1 atm, 300 K
Ground (collector)	Wall (13 W/m ²)
Canopy	Wall (0 W/m ²)
Chimney	Wall (0 W/m ²)

Quadrilateral grids were applied to all geometries (Figure 2c-i) and an inflation layer was used to predict the boundary layer profile near the wall and baffle (Figure 2c-ii). The values of y^+ are <5 for all geometries to ensure accurate prediction of the boundary layer. The grid density was determined by a grid independence test, in which the mass flow rate of the outlet was observed in relation to the number of grids (Figure 3). The grid independence test was performed with three different grid densities with 62,880 (Grid #1) to 123,720 (Grid #2) and 200,720 (Grid #3) grid numbers. The outlet mass flow rates of Grids #1 and #2 were 0.24% and 0.06% different from that of Grid #3, the densest grid, respectively. Therefore, to use computational power efficiently, for all cases in this study, a grid with the density similar to that of Grid #2 was used.

The convergence of the CFD model was determined by monitoring of the temperature and mass flow rate, which are important parameters for analysis (Figure 4). The mass flow rate monitored in the outlet was stable after the 10,000th iteration; the stable mass flow rate was measured as 0.1317 kg/s (Figure 4a). To confirm whether the temperature profile inside the SUT was fully developed, the average temperature in the SUT chimney inlet (green colored line in Figure 4b) was monitored. The temperature was found to be stable after the 10,000th iteration (Figure 4b). The converged value of the average temperature was 306.13 K. The computational result after 30,000 iterations, when the mass flow rate and temperature were sufficiently stabilized, was used for the analysis.

**Figure 3.** Mass flow rate in the SUT outlet for each grid case for grid independent test.

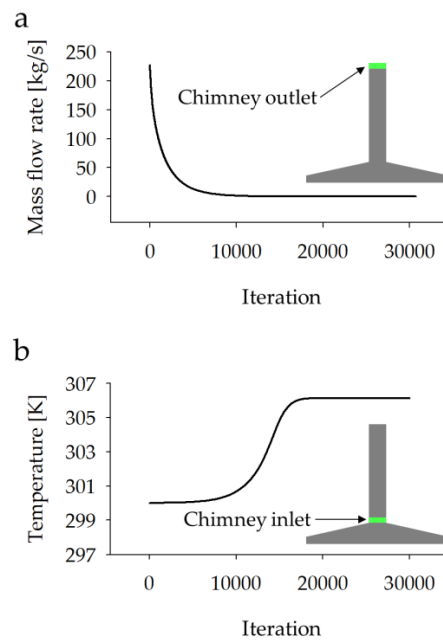


Figure 4. Monitoring of (a) the mass flow rate in the chimney outlet and (b) the average temperature in the chimney inlet.

3. Results and Discussion

Our CFD model was validated by comparison with experimental results [24] in terms of the temperature profile on the ground (blue colored arrow in Figure 5). In the experimental results, this temperature gradually increased as it approached the center axis (5 m in the x-coordinate, ground radius) on the ground; this tendency also appeared with our CFD model (red solid line, Figure 5). The temperature profile difference between the CFD and experimental results [24] was less than 3.2% (based on absolute temperature); the maximum error was calculated near the SUT inlet (at 0.25 m in the ground radius, Figure 5). This discrepancy can be explained as follows. Unlike the actual uneven heat flux emitted from the SUT ground, constant heat flux release was assumed in our CFD model. However, the fact that the error was less than 3.2% of the temperature prediction suggests that our CFD model is sufficiently useful to simulate the natural convection in an SUT.

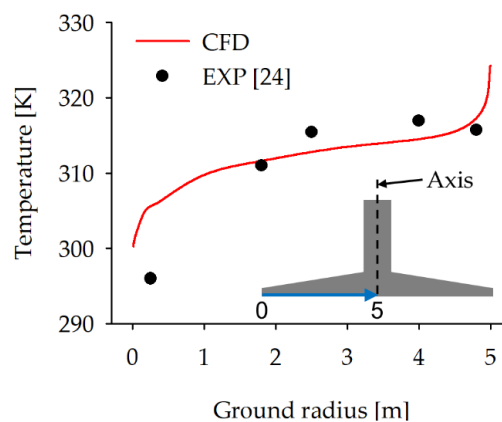


Figure 5. Comparison of the temperature profiles of computational fluid dynamics (CFD) and experimental results on the ground of collector (blue colored arrow).

Increased height of the baffle is beneficial for improved heat transfer; however, it has the negative effect of blocking the flow. Therefore, we tested three different baffle heights (Table 1) to observe the tendency of the flow and temperature profiles formed for each model. First, the flow fields (visualized as streamlines) of the SUT models were compared (Figure 6). In the Conv_SUT (the model without a baffle), two major flows were observed; one flow was the circulating streamlines in the collector of the SUT and the other was the streamlines flowing into the chimney (Figure 6a). The area of the circulation region (blue in Figure 6b,c), that is, a flow circulating in the collector by natural convection, was formed differently for each model with different heights. In comparison with the circulation region in the Conv_SUT (Figure 6b), the circulation regions in the SUT models with baffles were narrower (Figure 6c,d) owing to the baffle geometry; the higher the baffle, the narrower the circulation region. This tendency, which was observed regardless of the thermal boundary conditions of the baffle (adiabatic condition or heat flux condition), shows the negative effect of the baffle, that is, it reduces the cross-section, thus hindering the flow.

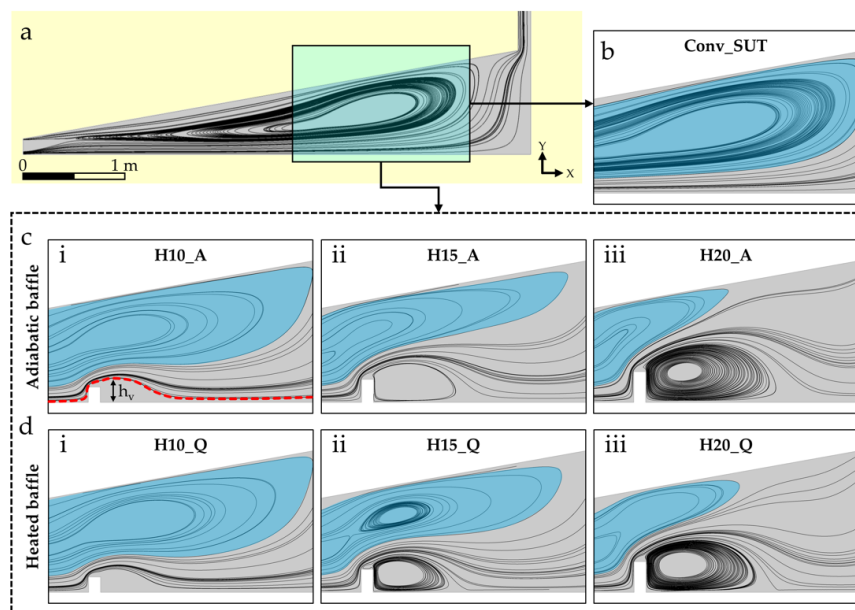


Figure 6. Flow field in the SUT models in relation to the baffle height. (a) Streamline of the Conv_SUT without a baffle. The rectangular area is to compare the streamlines of the models. (b) Streamline of the Conv_SUT in the rectangular area. The circulation flow is indicated by the blue area. (c) Streamline of the SUT models with adiabatic baffle; (i) H10_A, (ii) H15_A and (iii) H20_A. Note that the vortex height (defined as h_v) and the height of the streamline (red dashed line) formed just above the baffle. (d) Streamline of the SUT models with heated baffle (heat flux condition); (i) H10_Q, (ii) H15_Q and (iii) H20_Q.

However, regarding heat transfer, a baffle also has the positive effect of generating a vortex downstream of the baffle, enhancing the flow and thermal mixing. Through the streamlines shown in Figure 6c and d, it was observed that the size of the vortex was determined by the height of the baffle; the higher the baffle, the larger the vortex formed regardless of the thermal boundary conditions (adiabatic or heat flux conditions) of the baffle. The temperature contours show the effect of vortex size on the temperature distribution in the collector (Figure 7). In the Conv_SUT, in most areas, the temperature was under 306 K except near the ground (Figure 7a). In all SUT models with baffles (Figure 7b,c), the high-temperature region (>306 K) was widely distributed downstream of the baffle and this region was more widely distributed as the height of the baffle increased. Therefore, vortex size is important in determining the thermal distribution and the vortex size is again dependent on the baffle height. To quantify the vortex size in each model, the maximum height (h_v in Figure 6c–i) of the

streamline (red dashed line in Figure 6c–i) that passed over the baffle was measured and compared. Understandably, the vortex size (h_v) is proportional to the baffle height (Figure 8). First, in the models with adiabatic condition (blue bars, Figure 8, corresponding to the streamline results from Figure 6c), h_v of the H10_A was 0.158 m and h_v of H15_A and H20_A were 69.6% (0.268 m) and 154.4% (0.402 m) larger, respectively. Second, in the models with heat flux condition, h_v of H10_Q was 0.152 m and h_v of H15_Q and H20_Q were 61.8% (0.246 m) and 127.6% (0.346 m) larger, respectively (red bars, Figure 8, corresponding to the streamline results from Figure 6d). In addition, it was found that the h_v of models with an adiabatic baffle was larger than that of models with a heated baffle and the difference increased with increasing baffle height (up to 13.9% for H20 models) (Figure 8). This is because h_v is inversely proportional to the velocity of the flow that passes over the baffle; in other words, a higher velocity over the baffle suppresses vortex growth and vice versa. In the SUT with an adiabatic baffle (Figure 7b), the enhanced mixing of the heated air and the main flow was only due to the effect of the vortex, which means that the heat transfer efficiency was increased by the vortex only. On the other hand, in the SUT with a heated baffle, overall higher temperature distributions compared with those of the adiabatic baffle models were observed owing to the additional heat flux emitted from the baffle surface (Figure 7c). The results derived from the two antithetical assumptions of thermal condition show the range of possible phenomena in an actual situation, which is a compromise of these results shown in Figure 6b,c and Figure 7b,c.

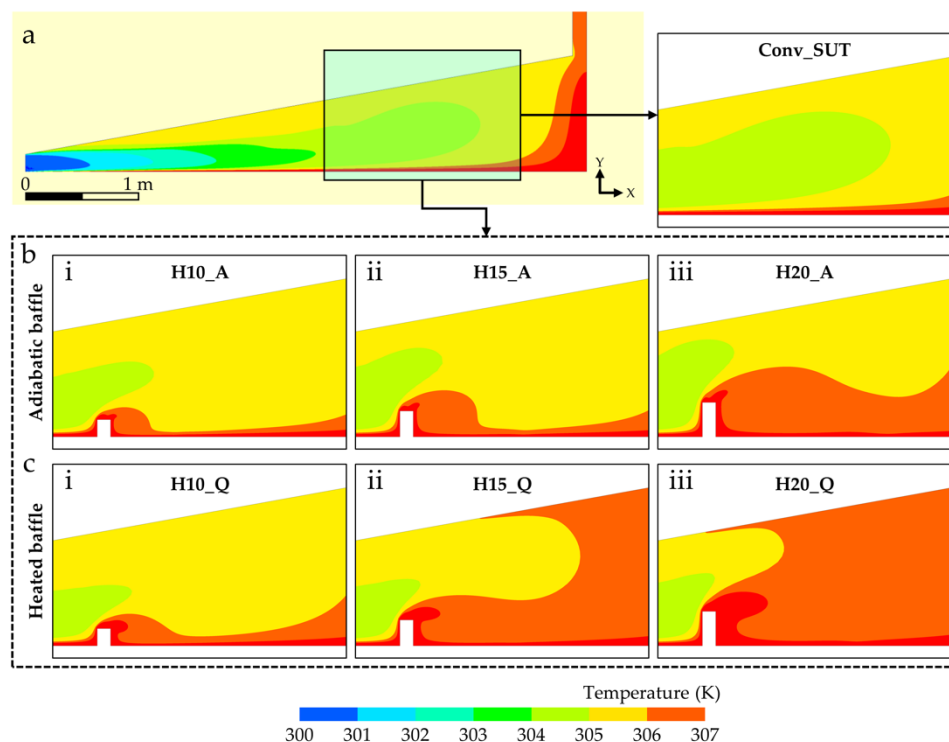


Figure 7. Temperature distribution in the SUT models according to the baffle height. (a) Temperature contour of the Conv_SUT without the baffle. The rectangular area is to compare the temperature contours of the models. (b) Temperature contour of the SUT models with adiabatic baffle; (i) H10_A, (ii) H15_A and (iii) H20_A. (c) Temperature contour of the SUT models with heated baffle (heat flux condition); (i) H10_Q, (ii) H15_Q and (iii) H20_Q.

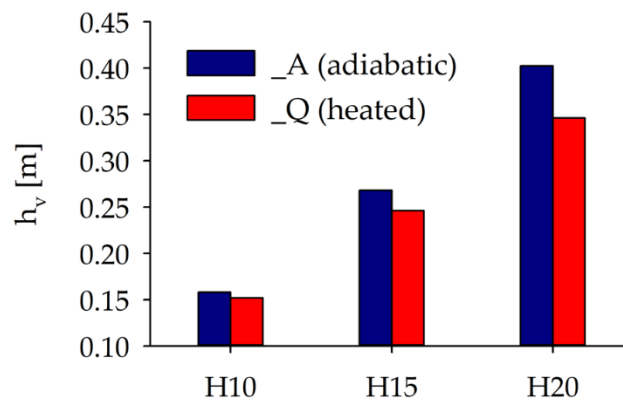


Figure 8. Comparison of vortex height (h_v) of the models with adiabatic baffle and heated baffle according to the baffle height. Blue bars represent adiabatic baffle models ('_A') and red bars represent heated baffle models ('_Q').

It is necessary to quantify how much the heat transfer from the ground to the main flow is enhanced by the vortex generated by the baffles with different heights. For this purpose, the temperature profiles were analyzed. The y-direction temperature profiles, along with the red line located 0.08 m downstream from the baffle, were derived for the seven models with various heights (Figure 9a). The characteristics of the temperature field can be summarized in the following three ways. First, the temperature profiles for the SUTs with baffles were generally higher than that for the Conv_SUT (black solid line, Figure 9a). Second, it was found that the higher the baffles, the higher the temperature profiles. Finally, the temperature distributions of the heated models were higher than those of the adiabatic models with the same heights (Figure 9a). The y-position of the peak temperature moved from 0.12 m (for H10) to 0.2 m (for H15) and 0.26 m (for H20) regardless of the thermal boundary conditions and the high-temperature region became wider in proportion to this position of peak temperature. The expansion of the high-temperature region led to an increased temperature difference with the air of the chimney outlet and strengthened the buoyancy, which is the driving force of an SUT. On the ground of the SUTs with baffles, the overall temperature profiles of these models were lower than that of the Conv_SUT and the general trend of the temperature profiles of all models increased as they approached the center of the SUT ($X = 2$ m in Figure 9b) with a few distinguishing features (Figure 9b). By the vortex flows (Figure 6c,d), the upper flow with lower temperature was dragged down to the ground and lower temperatures were found at this corresponding ground location (on the x-axis). This sudden decrease in temperature was observed as downward peaks of the temperature profile, as shown in Figure 9b. This location is determined by the size of the vortex identified via streamlines shown in Figure 6c,d. In the vortex region (shown in Figure 6c,d), the reverse-direction flow at the vortex bottom increases the temperature near the baffle ($X = 0$ m in Figure 9b) because this flow collects the heat transferred from the ground. The heat contained in the reverse-direction flow (generated by the vortex) is transferred to the main flow owing to the guidance of the baffle structure (see upper arrows, blocked flow, in Figure 1b–ii,iii). This is the mechanism by which the vortex contributes to the heat transfer of the SUT. The tendency of the temperature profiles in Figure 9a,b shows that the heat transfer in the SUT collector can be enhanced by modification of the baffle height.

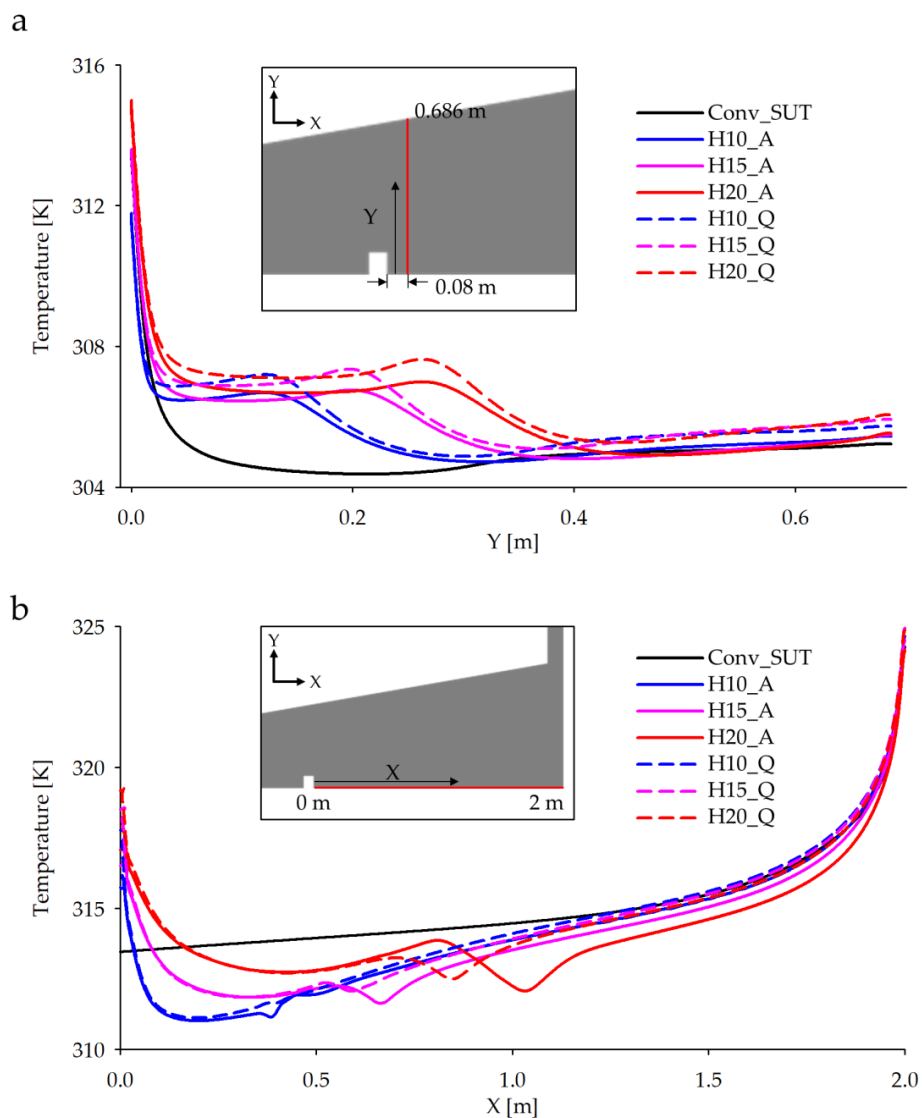


Figure 9. Temperature distribution downstream of the baffle. (a) Temperature profile along the line located 0.08 m from the baffle. (b) Temperature profile on the ground from the baffle to the center of the SUT.

In addition, we scrutinized the effects of various baffle widths and found that the baffle width had less influence on the flow field and temperature distribution than the baffle height. To confirm this, three more models (Table 1) were simulated and their streamlines and temperature contours in relation to variations of baffle width were compared (Figure 10). Despite the variations of baffle width, the vortex size downstream of the baffle was not significantly different. Therefore, the streamlines of W15_Q, W20_Q and W25_Q were similar to one another (Figure 10a). On the other hand, similar temperature contours were observed for each model (Figure 10b) because the vortex size, which is a parameter that determines the temperature distribution in the models, was similar. Thus, we concluded that the temperature distribution and flow field are mainly determined by the baffle height rather than the width.

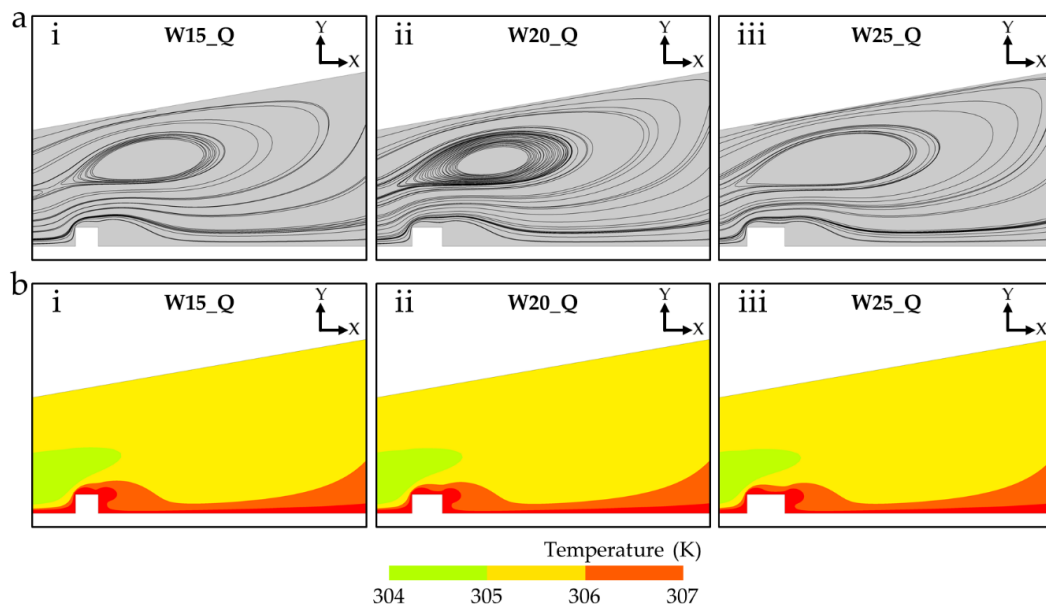


Figure 10. Effect of the baffle width on the flow field and temperature distribution. (a) Streamline of SUT models according to baffle width; (i) W15_Q, (ii) W20_Q and (iii) W25_Q. (b) Temperature contour of SUT models according to baffle width; (i) W15_Q, (ii) W20_Q and (iii) W25_Q.

The overall effect of various phenomena caused by baffles on SUT performance was analyzed by calculating kinetic power (Figure 11). The turbine output power is proportional to the kinetic energy of the wind passing through the chimney [3]. The available kinetic power (P) is calculated as

$$P = \rho AV^3 / 2, \quad (2)$$

where ρ is the density of air, A is the area of the cross-section through which the air passes and V is the velocity of the flow. The average velocities in the chimney inlet of all models (Table 1) were used to calculate the kinetic power of each model (Figure 11). In the baffle models of heat flux condition, the kinetic power increased linearly with baffle height (red bars in Figure 11a); the kinetic power increased by 3.01%, 3.83% and 4.69% in H10_Q, H15_Q and H20_Q, respectively, compared with that of the Conv_SUT. This increase in kinetic power is due to the additional heat transfer area created by the baffles as well as the vortex-based thermal-flow effect. Thus, it is necessary to compare it with the adiabatic baffle models to further investigate the benefits of baffle installation. The models with adiabatic baffles (blue bars in Figure 11a) showed less efficiency in terms of kinetic power. The kinetic power efficiency of H10_A and H15_A increased by 0.48% and 0.83%, respectively but decreased when the height of the baffle further increased to 0.2 m (H20_A). This is because the advantage of enhanced heat transfer generated by the vortex is offset by the disadvantage of the higher flow resistance caused by the baffle. In summary, baffles have two opposite effects; the positive/favorable effect is the increase in heat transfer by the vortex mechanism and the negative/unfavorable effect is the increase in flow resistance by narrowing the flow path in the collector. Thus, it is necessary to find the optimum baffle height to maximize the overall positive effect. Finally, the dependence of kinetic power on the baffle width was tested. As the baffle width increased (with heat flux condition), the kinetic power increased significantly compared with that of the Conv_SUT; however, the change in width resulted in a minimal increase in kinetic power (from 3.1% at W15_Q to 3.36% at W25_Q; Figure 11b). Note that the vortices formed in the models with width change were almost the same as those in models with various widths. This implies that the beneficial effect of vortices on heat transfer is the same for all models. Moreover, increased baffle width is less effective in increasing the overall heat transfer area compared with

increased baffle height, showing that the more efficient control parameter for determining the heat transfer area is the baffle height.

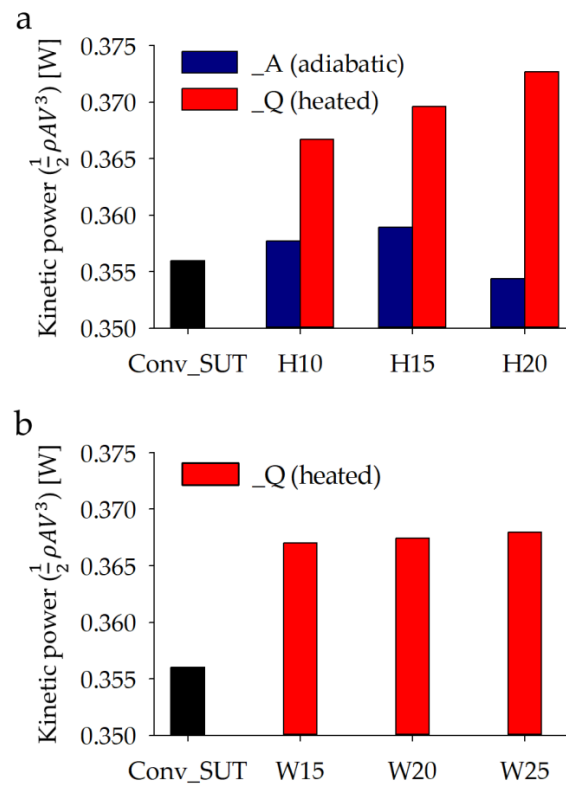


Figure 11. Kinetic power according to baffle height and width. (a) Kinetic power of the Conv_SUT and models with three different baffle heights. Blue bars represent adiabatic baffle models ('_A') and red bars represent heated baffle models ('_Q'). (b) Kinetic power of the Conv_SUT and models with three different baffle widths.

It should be noted that the two thermal boundary conditions for the baffle (adiabatic and heat flux conditions) are idealized conditions. In a real situation, the tradeoff between these two extreme situations must be examined carefully and applied appropriately to the design in order to achieve the optimal SUT systems under given thermo-fluid dynamic conditions.

4. Conclusions

In this study, numerical analysis was performed to confirm the effect of baffles on SUT performance. Two geometric parameters (baffle height and width) and the two thermal boundary conditions for the baffle (adiabatic condition and heat flux condition) were tested. The results showed two positive effects and one negative effect related to determining the kinetic power of an SUT with a baffle. The negative effect of the baffle is that it interferes with the flow. One of the positive effects of the baffle is the additional heat supply to the main flow due to the increase in heat transfer area; the other is the enhanced heat transfer efficiency due to the vortex generated downstream of the baffle. The reverse-direction flow at the vortex bottom, which draws heat from the ground, is guided by the baffle and supplies heat to the main flow. It has been also shown that baffle height has a greater effect than baffle width on SUT performance. In conclusion, to maximize the performance of the SUT, an optimized baffle design must be made that takes both positive and negative impacts into account. Our future work will pursue the comprehensive and optimized design of baffles to further improve SUT designs by adopting more geometric parameters other than the basic ones, whose effects were investigated in this study. A more efficient and systematic method to conduct such studies is the

19. Okada, S.; Uchida, T.; Karasudani, T.; Ohya, Y. Improvement in solar chimney power generation by using a diffuser tower. *J. Sol. Energy Eng.* **2015**, *137*. [[CrossRef](#)]
20. Gannon, A.J.; von Backström, T.W. Solar chimney turbine performance. *J. Sol. Energy Eng.* **2003**, *125*, 101–106. [[CrossRef](#)]
21. Von Backström, T.W.; Gannon, A.J. Solar chimney turbine characteristics. *Sol. Energy* **2004**, *76*, 235–241. [[CrossRef](#)]
22. Kirstein, C.F.; von Backström, T.W. Flow through a solar chimney power plant collector-to-chimney transition section. *J. Sol. Energy Eng.* **2006**, *128*, 312–317. [[CrossRef](#)]
23. Hu, S.; Leung, D.Y.C.; Chen, M.Z.Q.; Chan, J.C.Y. Effect of guide wall on the potential of a solar chimney power plant. *Renew. Energy* **2016**, *96*, 209–219. [[CrossRef](#)]
24. Nia, E.S.; Ghazikhani, M. Numerical investigation on heat transfer characteristics amelioration of a solar chimney power plant through passive flow control approach. *Energy Convers. Manag.* **2015**, *105*, 588–595. [[CrossRef](#)]
25. Fiebig, M.; Valencia, A.; Mitra, N.K. Wing-type vortex generators for fin-and-tube heat exchangers. *Exp. Therm. Fluid Sci.* **1993**, *7*, 287–295. [[CrossRef](#)]
26. Yoo, S.-Y.; Park, D.-S.; Chung, M.-H.; Lee, S.-Y. Heat transfer enhancement for fin-tube heat exchanger using vortex generators. *KSME Int. J.* **2002**, *16*, 109–115. [[CrossRef](#)]
27. Zeeshan, M.; Nath, S.; Bhanja, D.; Das, A. Numerical investigation for the optimal placements of rectangular vortex generators for improved thermal performance of fin-and-tube heat exchangers. *Appl. Therm. Eng.* **2018**, *136*, 589–601. [[CrossRef](#)]
28. Abdelatif, M.A.; Sayed Ahmed, S.A.E.; Mesalhy, O.M. Experimental and numerical study on thermal-hydraulic performance of wing-shaped-tubes-bundle equipped with winglet vortex generators. *Heat Mass Transf.* **2018**, *54*, 727–744. [[CrossRef](#)]
29. Han, Z.; Xu, Z.; Wang, J. Numerical simulation on heat transfer characteristics of rectangular vortex generators with a hole. *Int. J. Heat Mass Transf.* **2018**, *126*, 993–1001. [[CrossRef](#)]
30. Naik, H.; Tiwari, S. Effect of winglet location on performance of fin-tube heat exchangers with inline tube arrangement. *Int. J. Heat Mass Transf.* **2018**, *125*, 248–261. [[CrossRef](#)]
31. Alam, T.; Kim, M.-H. A comprehensive review on single phase heat transfer enhancement techniques in heat exchanger applications. *Renew. Sustain. Energy Rev.* **2018**, *81*, 813–839. [[CrossRef](#)]
32. Kumaresan, G.; Santosh, R.; Duraisamy, P.; Venkatesan, R.; Kumar, N.S. Numerical analysis of baffle cut on shell side heat exchanger performance with inclined baffles. *Heat Transf. Eng.* **2018**, *39*, 1156–1165. [[CrossRef](#)]
33. E, J.; Han, D.; Deng, Y.; Zuo, W.; Qian, C.; Wu, G.; Peng, Q.; Zhang, Z. Performance enhancement of a baffle-cut heat exchanger of exhaust gas recirculation. *Appl. Therm. Eng.* **2018**, *134*, 86–94. [[CrossRef](#)]
34. Fugmann, H.; Di Lauro, P.; Sawant, A.; Schnabel, L. Development of heat transfer surface area enhancements: A test facility for new heat exchanger designs. *Energies* **2018**, *11*, 1322. [[CrossRef](#)]
35. Ayadi, A.; Nasraoui, H.; Bouabidi, A.; Driss, Z.; Bsis, M.; Abid, M.S. Effect of the turbulence model on the simulation of the air flow in a solar chimney. *Int. J. Therm. Sci.* **2018**, *130*, 423–434. [[CrossRef](#)]
36. Ming, T.; Gui, J.; de Richter, R.K.; Pan, Y.; Xu, G. Numerical analysis on the solar updraft power plant system with a blockage. *Sol. Energy* **2013**, *98*, 58–69. [[CrossRef](#)]
37. Vieira, R.S.; Petry, A.P.; Rocha, L.A.O.; Isoldi, L.A.; dos Santos, E.D. Numerical evaluation of a solar chimney geometry for different ground temperatures by means of constructal design. *Renew. Energy* **2017**, *109*, 222–234. [[CrossRef](#)]
38. Ayadi, A.; Bouabidi, A.; Driss, Z.; Abid, M.S. Experimental and numerical analysis of the collector roof height effect on the solar chimney performance. *Renew. Energy* **2018**, *115*, 649–662. [[CrossRef](#)]
39. Ahsan, M. Numerical analysis of friction factor for a fully developed turbulent flow using $k-\epsilon$ turbulence model with enhanced wall treatment. *Beni-Suef Univ. J. Basic Appl. Sci.* **2014**, *3*, 269–277. [[CrossRef](#)]
40. Borgnakke, C.; Sonntag, R.E. *Fundamentals of Thermodynamics*, 8th ed.; John Wiley & Sons: Hoboken, NJ, USA, 2016.

